Destroy, create, transform and sublimate: laboratory dissociation studies on polycyclic aromatic hydrocarbons and analogues

Kamer, J.

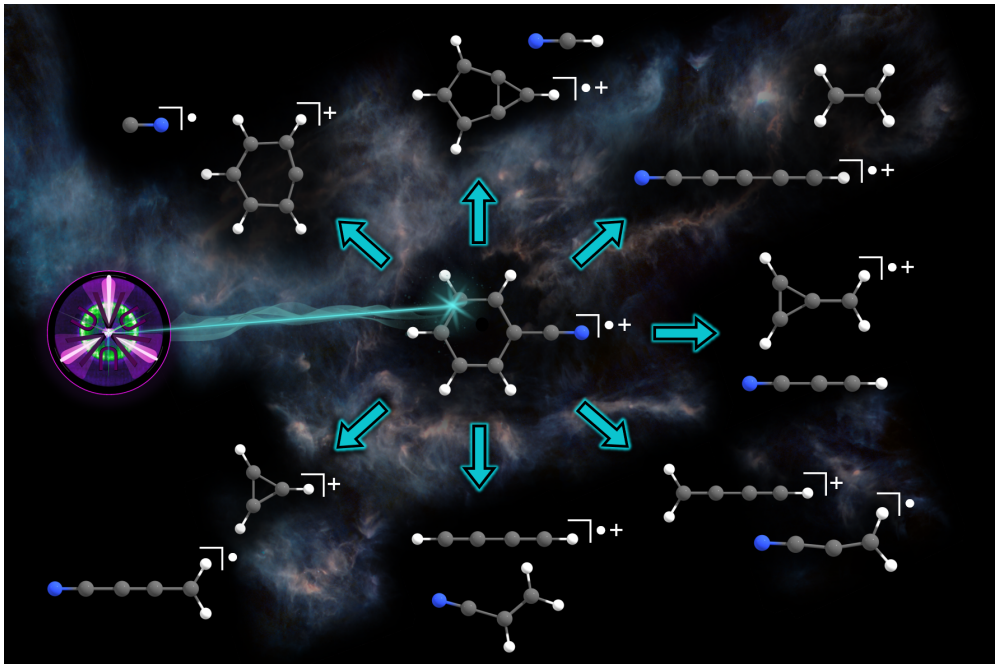

3 Threshold Photoelectron Spectrum and Dissociative Photoionization of Benzonitrile

The threshold photoionization and dissociative ionization of benzonitrile (C_6H_5CN) were studied using double imaging photoelectron photoion coincidence (i^2PEPICO) spectroscopy at the Vacuum Ultraviolet (VUV) beamline of the Swiss Light Source (SLS). The threshold photoelectron spectrum was recorded from 9.6 to 12.7 eV and Franck–Condon simulations of ionization into the ionic ground state, $\widetilde{X}^+$, as well as the $\widetilde{B}^+$ and $\widetilde{C}^+$ states were performed to assign the observed vibronic structures. The adiabatic ionization energies of the $\widetilde{X}^+$, $\widetilde{B}^+$ and $\widetilde{C}^+$ states are determined at (9.72 ± 0.02), (11.85 ± 0.03) and, tentatively, (12.07 ± 0.04) eV, respectively. Threshold ionization mass spectra were recorded from 13.75 to 19.75 eV and the breakdown diagram was constructed by plotting the fractional abundances of the parent ion and ionic dissociation products as a function of photon energy. The seven lowest energy dissociative photoionization channels of benzonitrile were found to yield $CN^\bullet$ + c-$C_6H_5{}^+$, HCN + $C_6H_4{}^{\bullet+}$, C_2H_4 + $HC_5N^{\bullet+}$, HC_3N + $C_4H_4{}^{\bullet+}$, $H_2C_3N^\bullet$ + $C_4H_3{}^+$, CH_2CHCN + $C_4H_2{}^{\bullet+}$ and $H_2C_4N^\bullet$ + c-$C_3H_3{}^+$. HCN loss from the benzonitrile cation is the dominant dissociation channel from the dissociation onset up to 18.1 eV and CH_2CHCN loss becomes dominant from 18.1 eV and up. We present extensive potential energy surface calculations on the $C_6H_5CN^{\bullet+}$ surface to rationalize the detected products. The breakdown diagram and time-of-flight mass spectra are fitted using a Rice–Ramsperger–Kassel–Marcus statistical model. Anchoring the fit to the CBS-QB3 result (3.42 eV) for the barrier to HCN loss, we obtained experimental dissociation barriers for the products of 4.30 eV (CN loss), 5.53 eV (C_2H_4 loss), 4.33 eV (HC_3N loss), 5.15 eV (H_2C_3N loss), 4.93 eV (CH_2CHCN loss) and 4.41 eV (H_2C_4N loss). We compare our work to studies of the electron-induced dissociative ionization of benzonitrile and isoelectronic phenylacetylene (C_8H_6), as well as the VUV-induced dissociation of protonated benzonitrile ($C_6H_5CNH^+$). Also, we discuss the potential role of barrierless association reactions found for some of the identified fragments as a source of benzonitrile$^{(\bullet+)}$ in interstellar chemistry and in Titan's atmosphere.

Kamer, J., Schleier, D., Donker, M., Hemberger, P., Bodi, A., Bouwman, J., 2023, Physical Chemistry Chemical Physics, 25, 29070-29079.

3.1 Introduction

Polycyclic aromatic hydrocarbons (PAHs) are generally accepted to be the carriers of the aromatic infrared bands (AIBs), which comprise ubiquitous infrared (IR) emission features observed towards a variety of interstellar environments (Allamandola *et al.* 1985, 1989; Leger & Puget 1984; Tielens 2008). Nitrogen-containing PAH species, also known as the polycyclic aromatic nitrogen heterocycles (PANHs), have also been hypothesized to contribute to the IR emission bands (Hudgins *et al.* 2005; Tielens 2008). The broad AIBs only allow for PAHs to be assigned as a class of molecules and it took until 2001 for the first unambiguous identification of an aromatic molecule in the interstellar medium, benzene, to be made. Benzene (c-C_6H_6) was identified through Infrared Space Observatory observations of its IR ν_4 vibrational mode at 14.84 μm towards protoplanetary nebula CRL 618 (Cernicharo *et al.* 2001). Benzene is thought to be an important precursor in the bottom-up formation of PA(N)H species (Reizer *et al.* 2022; Frenklach 2002; Parker *et al.* 2012; Parker & Kaiser 2017; Comandini & Brezinsky 2011).

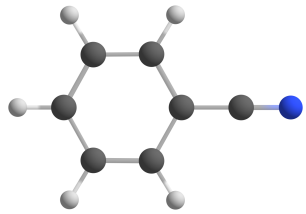

Figure 3.1: Molecular structure of benzonitrile (C_6H_5CN).

Individual identification of aromatic compounds in the ISM using Earth-based telescope observations of their IR features is challenging because of the limited IR transmission window of the atmosphere (Cooke *et al.* 2020). Moreover, the assignment of complex molecules based on infrared transitions is hampered by the lack of molecular specificity of IR transitions. Therefore, the focus shifted to searching for interstellar aromatics using radio astronomical observations. However, this requires the molecule to have a permanent dipole moment. The first aromatic molecule to be detected using radio astronomy was the polar benzonitrile (C_6H_5CN, Fig. 3.1) (Cooke *et al.* 2020). It was first detected in Taurus Molecular Cloud (TMC-1) in 2018 (McGuire *et al.* 2018) and later, in 2021, towards molecular clouds Serpens 1A, Serpens 1B, Serpens 2 and MC27/L1521F (Burkhardt *et al.* 2021a). Benzonitrile is considered to be a tracer of benzene (Cooke *et al.* 2020), as it is thought to form via the barrierless radical–neutral reaction (Trevitt *et al.* 2010; Loison *et al.* 2019; Cooke *et al.* 2020):

$$CN^{\bullet} + C_6H_6 \longrightarrow C_6H_5CN + H. \tag{3.1}$$

Moreover, it has been suggested that benzonitrile is a precursor species in the bottom-up formation of PA(N)Hs in the ISM (McGuire *et al.* 2018; Jacovella *et al.* 2022a).

Benzonitrile has also been suggested to play a role in the chemistry of the atmosphere of Saturn's largest moon Titan. By mixing CH_4, NH_3 and H_2O in a spark-discharge synthesis experiment, complex hydrocarbons are formed, commonly referred to as tholins, including benzonitrile (Khare *et al.* 1981). Based on model predictions, the benzonitrile mole fraction in Titan's atmosphere reaches 1.5×10^{-9} at an altitude of 1000 km (Loison *et al.* 2019).

Vacuum ultraviolet (VUV) radiation drives chemistry in interstellar environments, such as photodissociation regions (PDRs), molecular clouds, circumstellar envelopes and circumstellar disks (Tielens & Hollenbach 1985; Hollenbach & Tielens 1999). Molecules absorbing a VUV photon can photodissociate or (dissociatively) ionize. Ionization of benzonitrile has been studied in the past and its ionization energy (IE) was determined at 9.73 eV (Araki *et al.*

1996; Kobayashi & Nagakura 1974; Watanabe *et al.* 1962). VUV radiation of this energy is not absorbed by abundant molecular and atomic hydrogen (Draine 1978; Mathis *et al.* 1983) and thus cationic benzonitrile may be present in the ISM as well, and could subsequently dissociate upon further absorption of photons. The energy-dependent dissociative ionization mechanism of benzonitrile can provide input for astrochemical and atmospheric chemistry models and reveal the role of this aromatic molecule in these environments.

In the 1980s, electron ionization (EI) studies of benzonitrile showed that HCN is the dominant neutral fragment in dissociative ionization (Inoue *et al.* 1983; Burgers *et al.* 1984; Molenaar-Langeveld *et al.* 1986), resulting in $C_6H_4^{\bullet+}$ (m/z 76) as the cationic co-fragment. Mass spectra measured by Molenaar-Langeveld *et al.* (1986) also revealed m/z 50 ($C_4H_2^{\bullet+}$ or C_3N^+) as a major dissociation channel, accompanied by the loss of neutral C_3H_3N or $C_4H_5^{\bullet}$, respectively. Without energetics data and because of the insufficient mass resolution, neither could these channels be distinguished nor the fragment structures be established.

A recent study utilized infrared predissociation (IRPD) spectroscopy to characterize the structures of the ionic fragments formed from electron-induced dissociative ionization of benzonitrile (Rap *et al.* 2023). The dominant HCN/HNC loss, at an electron energy of 15 eV, was found to result in *ortho*-benzyne$^{\bullet+}$ and bicyclic *meta*-benzyne$^{\bullet+}$ (BMB$^{\bullet+}$) $C_6H_4^{\bullet+}$ fragment ions. The latter was only found to be a minor contributor to the spectrum. The dissociation pathways to both isomers were calculated using density functional theory (DFT) with the B3LYP-GD3 functional and the double-ζ N07D basis set. The rate-limiting transition state to BMB$^{\bullet+}$ was found to be a H atom transfer from a neighbouring CH to the nitrogen atom. This transition state also happens to be the highest lying transition state in the formation pathway of *ortho*-benzyne$^{\bullet+}$. However, the energy of the *ortho*-benzyne$^{\bullet+}$ + HCN/HNC fragments exceeds the energy of this transition state and the formation of *ortho*-benzyne$^{\bullet+}$ proceeds without a reverse barrier. At an electron energy of 50 eV, the IRPD spectra for the m/z 77 and 75 ions could be assigned to the phenylium$^+$ (*c*-$C_6H_5^+$) and cyanodiacetylene$^{\bullet+}$ ($HC_5N^{\bullet+}$) ions, formed by the loss of $CN^{\bullet}$ and C_2H_4, respectively. Surprisingly, the m/z 50 peak, reported to be a major fragment ion by Molenaar-Langeveld *et al.* (1986), was not observed (Rap *et al.* 2023).

The dissociation mechanisms of species related to benzonitrile have also gained considerable attention. For example, the VUV photodissociation of protonated benzonitrile ($C_6H_5CNH^+$) was measured by Jacovella *et al.* (2022a) between 4.5 and 13.6 eV photon energy using ion trap mass spectrometry and interpreted with the help of CBS-QB3 calculations. Protonated benzonitrile dissociates to form the phenylium cation (*c*-$C_6H_5^+$) and 3-methylcyclopropene cation ($C_4H_5^+$) by the loss of the hydrogen (iso)cyanide (HCN or HNC) and cyanoacetylene (HC_3N), respectively. Dyakov *et al.* (2020) studied the dissociative ionization of phenylacetylene – which is isoelectronic with benzonitrile – and explored the $C_8H_6^{\bullet+}$ potential energy surface (PES). One of the energetically accessible channels was found to be isomerization to benzocyclo-butadiene$^{\bullet+}$ (BCB$^{\bullet+}$) followed by the formation of *meta*-benzyne$^{\bullet+}$ via C_2H_2 loss. The isomerization can proceed via a single transition state from phenylacetylene$^{\bullet+}$, and via a second pathway that contains an additional intermediate state. The latter pathway is the lowest in energy and also analogous to the suggested pathway by Rap *et al.* (2023) for HCN/HNC loss of benzonitrile$^{\bullet+}$.

In this work, we study the unimolecular dissociation of cationic benzonitrile after VUV photoionization. To accomplish this, we employ the double imaging photoion photoelectron coincidence (i^2PEPICO) technique in the photon energy range from 9.5 to 19.75 eV. This method allows us to construct a breakdown diagram by plotting the fractional abundances of benzonitrile$^{\bullet+}$ and its dissociative ionization fragment ions observed in threshold ionization mass spectra as a function of the VUV photon energy. Furthermore, we also recorded the threshold photoelectron spectrum (TPES) of the parent molecule. We first present the TPES and investigate it using computational chemistry methods combined with Franck–Condon simulations to gain insight into the electronic structure of benzonitrile. Guided by the breakdown diagram, the benzonitrile$^{\bullet+}$ breakdown diagram is shown and, guided by the

breakdown diagram, the benzonitrile$^{\bullet+}$ potential energy surface (PES) is explored computationally to identify the dissociation pathways. Subsequently, a Rice–Ramsperger–Kassel–Marcus (RRKM) statistical model is used to determine the barriers to the experimentally observed fragmentation channels. The findings reported here are placed in context by comparing the results to the dissociation of (protonated) benzonitrile as well as the dissociative ionization of the isoelectronic phenylacetylene. Finally, the astrochemical implications of our findings are discussed.

3.2 Methods

3.2.1 Experimental

The experiments were conducted using the i^2PEPICO endstation at the VUV beamline of the Swiss Light Source at Paul Scherrer Institute. The beamline and i^2PEPICO endstation will be described briefly and a more detailed description is given elsewhere (Johnson *et al.* 2009; Bodi *et al.* 2012; Sztáray *et al.* 2017).

Benzonitrile (C_6H_5CN) was purchased from Sigma–Aldrich ($\geq$ 99%) and used without further purification. The vapor from the headspace of the room-temperature sample container was admitted to the i^2PEPICO ionization region through Teflon tubing. A needle valve was used to control the flow of benzonitrile such that the stagnation pressure in the vacuum chamber was about 10^{-6} mbar. The neutral benzonitrile was intersected with the monochromatic radiation from the VUV beamline. The photon energy was scanned between 9.5 and 19.75 eV with step sizes ranging between 5 and 50 meV.

Photoelectrons and photoions were extracted using a 105 $\mathrm{V\,cm^{-1}}$ and 143 $\mathrm{V\,cm^{-1}}$ static electric field for the energy range 9.5 to 15.7 eV and 15.7 to 19.75 eV, respectively. Electrons were velocity map imaged onto a RoentDek delay-line anode imaging detector, and their arrival time provided the start signal for the time-of-flight (TOF) analysis of the coincident photoions. These were space focused onto a second RoentDek imaging delay-line detector, and their arrival time provides information on their mass-to-charge ratio (m/z). Due to the low extraction field and the long extraction region, cations have a long residence time in the acceleration region. If a dissociation is not instantaneous but takes place on the extraction timescale, typically within a few microseconds, the recorded mass spectrum will reveal broad and asymmetric daughter ion TOF peak shapes. The shape of the daughter ion peaks is used to determine the dissociation rate in the 10^3–10^7 $\mathrm{s^{-1}}$ range. Modeled rates are then fitted to the experimental data by varying the barriers to dissociation and scaling the transitional frequencies using the ion optics parameters (Bodi *et al.* 2009). Thus, the kinetic shift is accounted for in the model and accurate dissociation barrier heights are derived.

Threshold electrons were imaged onto the center of the electron imaging detector with an energy resolution better than 1 meV. "Hot" electrons, i.e. electrons with non-zero kinetic energy but with a negligible lateral velocity component are also imaged onto the center spot of the detector, and their contribution is subtracted as described in the literature (Sztáray *et al.* 2017). A photoion mass-selected threshold photoelectron spectrum (ms-TPES) of benzonitrile is constructed by plotting the integrated ion signal at m/z 103, coincident with threshold electrons, as a function of photon energy. Furthermore, above the dissociative ionization threshold, the breakdown diagram of benzonitrile is constructed by plotting the fractional abundances of the integrated signals of the parent and daughter ion signals coincident with threshold electrons as a function of photon energy, i.e as a function of internal energy of the benzonitrile cation.

3.2.2 Computational

Density functional theory (DFT) calculations and geometry optimizations were performed using the Gaussian16 (Frisch *et al.* 2016) program. To simulate the TPES, Franck–Condon factors were computed in the double harmonic approximation using the program eZspectrum (Gozem & Krylov 2022) which takes the DFT optimized geometries and vibrational wavefunctions of the neutral and (electronically excited) cationic species as input. Franck–Condon factors of ionization to the excited states are calculated based on the time-dependent density functional theory (TD-DFT) optimized structure of the excited ionic states, calculated using the ωB97-XD/6-311++G(d,p) method. The resulting stick spectra are convolved with a Gaussian profile with a full-width half maximum (FWHM) of 25 meV to allow for a comparison with the experimental TPES data. The adiabatic ionization energy of benzonitrile is determined from the maximum of the measured origin transition of the TPES, and the error bar is established as the half-width-at-half-maximum of the origin transition.

In order to determine the dissociation barriers and to elucidate the structures of the ionic and neutral dissociative ionization products, the PES was explored at the B3LYP/6-311++G(d,p) level. Transition states and intermediate states were located using the B3LYP functional and subsequently refined by the CBS-QB3 composite method (Montgomery *et al.* 1999, 2000). The miniPEPICO modeling program by Sztáray *et al.* (2010) was utilized to model the breakdown diagram and to simultaneously fit the measured time-of-flight mass spectra. The computed vibrational modes of neutral benzonitrile and the rate-determining transition states combined with experimental parameters, such as sample temperature and ion optics configuration, provide the input for the program. Rigid activated complex (RAC) Rice-Ramsperger-Kassel-Marcus (RRKM) theory is used to calculate the rate curves as a function of internal energy. This, in combination with the fitted barrier heights and transitional frequencies of the rate-determining states, is used to reproduce the experimental data.

3.3 Results

3.3.1 Threshold photoelectron spectroscopy

Figure 3.2 shows the threshold photoelectron spectrum (TPES) of benzonitrile for the 9.6–10.4 eV photon energy range. The peak at (9.72 ± 0.02) eV is attributed to the origin transition into the cationic ground state $\widetilde{X}^+\ ^2B_1$, which corresponds to ionization out of the highest occupied molecular orbital (HOMO) of the neutral. The (9.72 ± 0.02) eV is consequently assigned to the adiabatic ionization energy (IE_{ad}), which is in agreement with the previously determined IE_{ad} of (9.7315 ± 0.0002) eV (Araki *et al.* 1996), and our CBS-QB3-computed $IE_{ad} = 9.78$ eV. The origin transition is the most intense peak of this electronic state, pointing towards a small geometry change in benzonitrile upon ionization. The vibronic progression exhibits a peak at 9.78 eV ($480\,cm^{-1}$ above the origin transition) which arises mostly from a 5_0^1 vibrational transition, corresponding to a ring stretching mode computed at $459\,cm^{-1}$. Furthermore, the rising slope starting at 9.8 eV is matched well by the simulated peak at 9.82 eV ($810\,cm^{-1}$ above the origin transition) and is attributed to a 9_0^1 vibrational transition. This transition corresponds to a ring stretching mode computed at $754\,cm^{-1}$. Aside from these fundamental transitions, the vibrational structure is rather convoluted due to the large number of transitions with similar intensities and no further peaks can be assigned unambiguously. Despite this, the Franck–Condon simulation reproduces the experimental spectrum well, and discrepancies arise mostly at higher energies (>10.0 eV), which could be explained by the presence of the cationic first excited state $\widetilde{A}^+$ ($^2A_2$). The TPES in this energy range clearly exhibits a shoulder, however, fine structures are absent, which is likely caused by lifetime broadening. Geometry optimizations for the $\widetilde{A}^+$ state were unsuccessful. This is suggestive of state mixing, which might explain the broadening. We calculated a

vertical ionization energy for the $\widetilde{A}^+$ state of 10.12 eV. This value is comparable to an earlier assignment of the $\widetilde{A}^+$ state at 10.17 eV by Kimura *et al.* (1981).

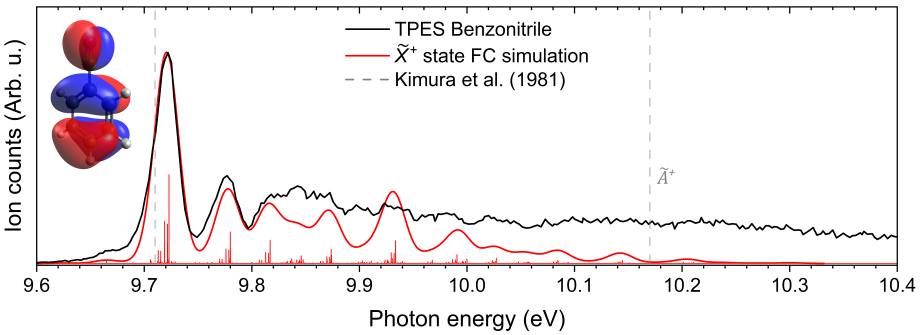

Figure 3.2: Threshold photoelectron spectrum of benzonitrile (black) for the energy range from 9.6 to 10.4 eV, together with the simulated Frank–Condon spectrum for the ground state ($\widetilde{X}^+$, red) ion. The dashed lines indicate the assignments made by Kimura *et al.* (1981) The $\widetilde{X}^+$ state corresponds to the ionization out of the HOMO of neutral benzonitrile, which is presented on the top-left.

Figure 3.3 shows the TPES of benzonitrile for the energy range spanning from 11.5 to 12.7 eV. Several distinct features are seen in the TPES starting around 11.8 eV. The energy of the $\widetilde{B}^+$ and $\widetilde{C}^+$ excited states was calculated using TD-DFT at the ωB97-XD/6-311++G(d,p) level to be 2.08 eV and 2.57 eV above the cationic ground state, respectively. Combined with the known IE to the ground cation state, this yields IEs of 11.80 eV for the $\widetilde{B}^+$ state and 12.29 eV for the $\widetilde{C}^+$ state. The former coincides with a strong resonance in the TPES. Furthermore, Xu *et al.* (2006) showed that the benzonitrile $\widetilde{B}^+$ state lies 2.14 eV above the cationic ground state, i.e., at 11.86 eV. Thus, we attribute the TPES peak at 11.85 eV to ionization into the $\widetilde{B}^+$ $^2B_2$ state by removal of a HOMO−2 electron. Both $\widetilde{B}^+$ and $\widetilde{C}^+$ states are amenable to TD-DFT geometry optimization and Franck–Condon simulation. This shows, similar to ionization into the ionic ground state, the origin transitions to be most intense, thanks to the small geometry change. The sum of the two traces reproduces the experimental spectrum best if the the TPES feature at 12.07 eV is assigned at the origin transition to the $\widetilde{C}^+$ $^2B_1$ state by the removal of a HOMO−3 electron from neutral benzonitrile. Aside from the high-energy shoulder, due to ionization to the $\widetilde{B}^+$ state, the assignment is driven by the peak around 12.19 eV in the TPES in Fig. 3.3, which is predicted to be dominated by a transition in the $\widetilde{C}^+$ state. For the $\widetilde{B}^+$ state, the experimental value agrees well with the computation, while the difference is −0.22 eV for the $\widetilde{C}^+$ state. The adiabatic ionization energy of the $\widetilde{B}^+$ is, thus, determined to be (11.85 ± 0.03) and we tentatively assign the $\widetilde{C}^+$ state adiabatic ionization energy as (12.07 ± 0.04) eV. Besides strong coupling between the $\widetilde{B}^+$ and $\widetilde{C}^+$ states and the resulting lifetime broadening, anharmonic effects and the different electronic transition dipole moments may also account for differences between the measured and the FC-simulated TPES.

3.3.2 TOF mass spectra and breakdown diagram

Threshold photoelectron photoion coincidence mass spectra were measured over the photon energy range spanning from 13.75 to 19.75 eV. Photon energy step sizes of 25 meV were used for the 13.75 eV to 15.7 eV range and 50 meV step sizes were applied from 15.7 eV onward. A representative selection of eight threshold mass spectra of the dissociative ionization of benzonitrile normalized to the highest peak is presented in Fig. 3.4.

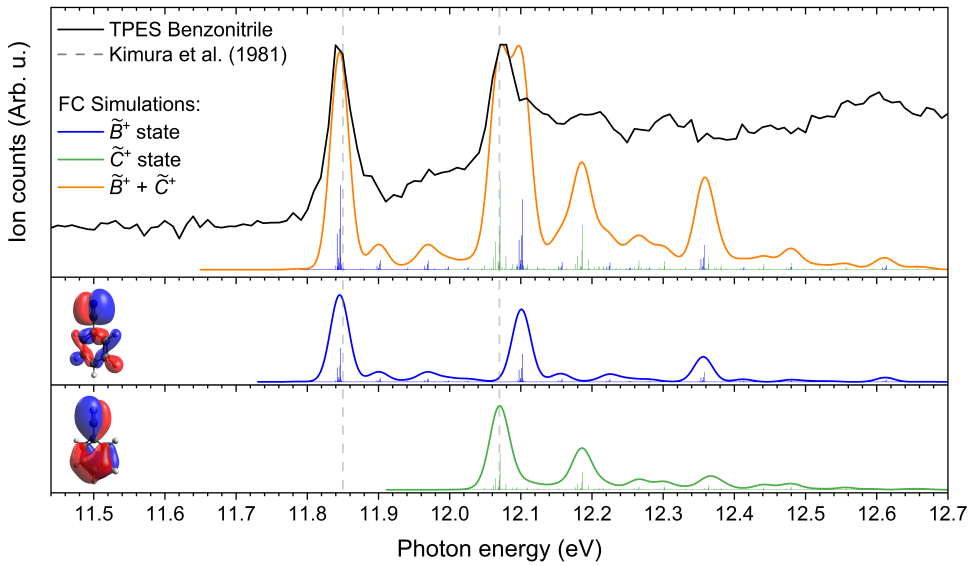

Figure 3.3: Threshold photoelectron spectrum of benzonitrile (black) for the energy range of 11.5 to 12.7 eV, together with the simulated Frank–Condon spectra for the second ($\widetilde{B}^+$, blue) and third ($\widetilde{C}^+$, green) electronically excited ion state. The orange line represents the aggregated Frank–Condon spectra of the second and third electronically excited ion states. The dashed lines indicate the assignments made by Kimura *et al.* (1981) The $\widetilde{B}^+$ and $\widetilde{C}^+$ states correspond to the ionization out of the HOMO−2 and HOMO−3 of neutral benzonitrile, respectively. These are presented on the left of the spectra of each respective state.

The main dissociation products in the photon energy up to 19.75 eV are m/z 77, 76, 75, 52, 51, 50 and 39. Ion signals are also detected at m/z 102 (H loss), 64 and 63. However, these signals are not considered in the analysis since their fractional abundance is small ($\leq 10\%$). The asymmetric peak shape of m/z 76 in Fig. 3.4 close to its appearance in the mass spectra at low energies is indicative of the slow dissociation of an activated ion. At 15.7 eV photon energy, the benzonitrile cation internal energy is high enough for it to promptly fragment in the ionization region, resulting in a symmetric fragment ion peak shape in the mass spectrum.

Fractional abundances of the benzonitrile and its fragment ions are plotted in the breakdown diagram in Fig. 3.5. The m/z 76 signal is integrated over its full width, i.e. from m/z 75.5 to 84, over the photon energy range from 13.75 to 15.7 eV to account for the asymmetry in the peak shape at low energies and integrate the full ion signal. From 15.7 eV onward the signal is integrated from m/z 75.5 to 76.5 as the peak is now symmetric. The latter ensures that the m/z 75 and 77 signals that are also present at these higher energies are not included in the integration of the m/z 76 signal.

The fractional abundance of m/z 77 at 15.7 eV is determined to be 18%. At lower energies the m/z 77 signal is masked by the overlapping asymmetric m/z 76 peak. As the fragment ion peak shape is characteristic of the depletion rate of the metastable parent ion, both peaks will have similar shapes, and the broad but less intense m/z 77 peak is poorly resolved and cannot be integrated or fitted reliably. To construct a realistic breakdown diagram, we assume smoothly changing branching ratios between the two channels, and the m/z 77 fractional abundance is extrapolated between 14.7 and 15.7 eV based on the data between 15.7 and 16.7 eV. This is illustrated in Fig. 3.5 by open, blue circles. A 1σ scatter was also added to ensure that this range does not overly influence the overall goodness of fit in the

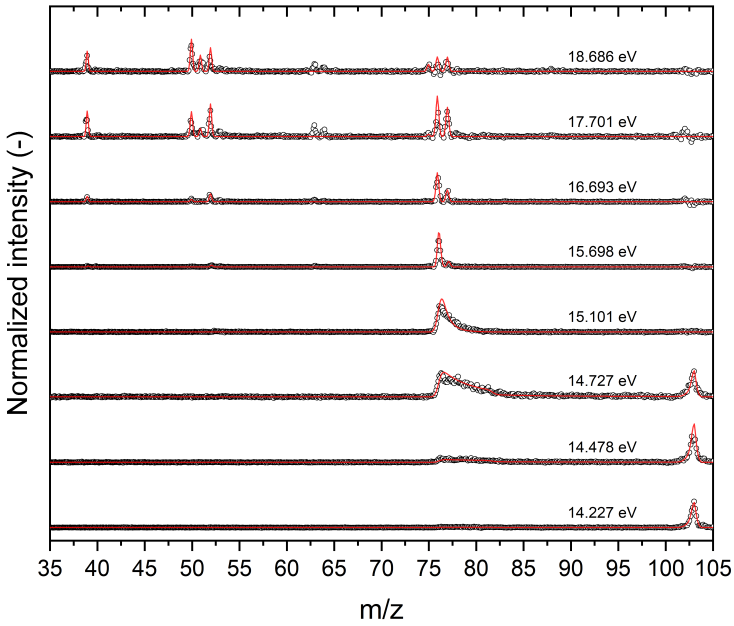

Figure 3.4: Normalized threshold photoelectron photoion coincidence mass spectra of benzonitrile at representative photon energies (open circles), accompanied by modeled fits (red lines).

optimization. The fractional abundances have been adjusted for the natural abundances of ^{13}C and ^{15}N isotopes of 1.109% and 0.36%, respectively.

Interestingly, and despite the wide energy range studied, the ionic fragments do not disappear at higher photon energies after their onset as they are not depleted by sequential fragmentation steps. Furthermore, the slowly diminishing fractional abundance of the initially dominant ionic fragments is also indicative of competing parallel channels instead of sequential fragmentation steps. This suggests that all ionic fragments result from parallel dissociation pathways and is a testament to the stability of the primary fragment cations.

3.3.3 Potential energy surface

Relaxed bond length and angle scans were performed at the B3LYP/6-311++G(d,p) level of theory to locate transition states, intermediates and products on the PES. Subsequently, the energies of the stationary points and transition states were refined at the CBS-QB3 level of theory. A summary of the PES leading to the main dissociative ionization products is shown in Fig. 3.6. Here, a concise description of the pathways is provided in descending order of their contribution to the breakdown diagram. Zero-point corrected energies are relative to the benzonitrile cation. Further details on the PES can be found in Figs. 3.13-3.19 in the appendix.

HCN loss (m/z 76 product ion) is the dominant dissociation channel from the dissociative ionization onset up to about 18.1 eV. At 15.0 eV, the fragment ion accounts for a total of 98% of the threshold ionization signal and then tapers off. This channel leads to the formation of bicyclic *meta*-benzyne$^{\bullet+}$ (BMB$^{\bullet+}$) and HCN at 3.29 eV. The lowest energy path starts with H atom transfer from one of the vicinal CH groups to the N atom at a

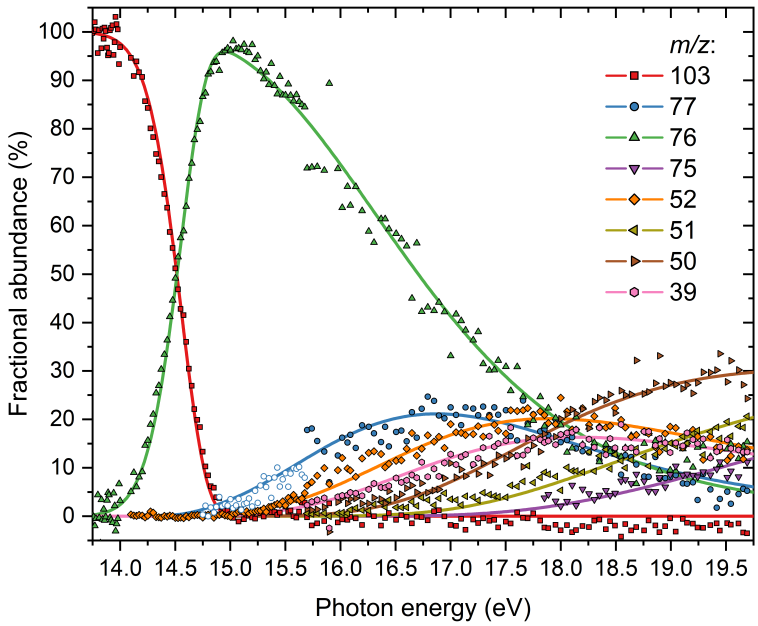

Figure 3.5: Measured breakdown diagram of benzonitrile (symbols) shown together with the fitted model (solid lines). The open, blue circles depict the extrapolated m/z 77 signal between the photon energies of 14.7 and 15.7 eV based on the data between 15.7 and 16.7 eV (see text).

transition state energy of 3.42 eV. This also happens to be the rate-limiting step of the HCN loss channel. Another possible product channel leads to the monocyclic *meta*-benzyne$^{\bullet+}$ + HCN at 3.41 eV. A computational study using the CBS-QB3 composite method by Jacovella *et al.* (2022b) has shown that the BMB$^{\bullet+}$ isomer is thermodynamically favoured over the monocyclic *meta*-benzyne$^{\bullet+}$. However, CASPT2 (Li & Huang 2008) and CASSCF (Nguyen *et al.* 2005) calculations reported the two isomers to be almost degenerate. The singly occupied molecular orbitals (SOMOs) of *meta*-benzyne$^{\bullet+}$ and BMB$^{\bullet+}$, presented in appendix Fig. 3.20, are of $^2A_1$ and $^2A_2$ symmetry, respectively. Thus, the two *meta*-benzyne$^{\bullet+}$ isomers represent minima with different wave function symmetries and are therefore discernible even if they are almost isoenergetic and are connected only by ring-deformation. We will present BMB$^{\bullet+}$ as the initial product of HCN loss, as it is perhaps energetically favorable. Nevertheless, both channels have final products with calculated energies below the rate-limiting transition state (3.42 eV), and the formation of both BMB$^{\bullet+}$ and *meta*-benzyne$^{\bullet+}$ is energetically allowed. *Ortho*-benzyne$^{\bullet+}$ + HCN may also be formed in this channel at a computed threshold of 3.71 eV. This is 0.29 eV higher than the calculated energy of the rate-limiting transition state for the formation of BMB$^{\bullet+}$ or *meta*-benzyne$^{\bullet+}$ via HCN loss. As such, *ortho*-benzyne$^{\bullet+}$ is an unlikely product at the appearance energy of this fragment ion peak but may be formed at higher internal energies.

Hydrogen isocyanide, HNC, loss is an isomeric neutral fragment leading to the same m/z 76 fragment ion. It is less stable than HCN by 0.65 eV (Ruscic *et al.* 2004, 2005), similar to the computed energy difference of 0.61 eV. While HNC is energetically inaccessible at the onset of dissociative ionization, HNC loss only requires two hydrogen migration steps to yield *meta*-benzyne$^{\bullet+}$, and only one to yield *ortho*-benzyne$^{\bullet+}$. Thus, the less constrained reaction

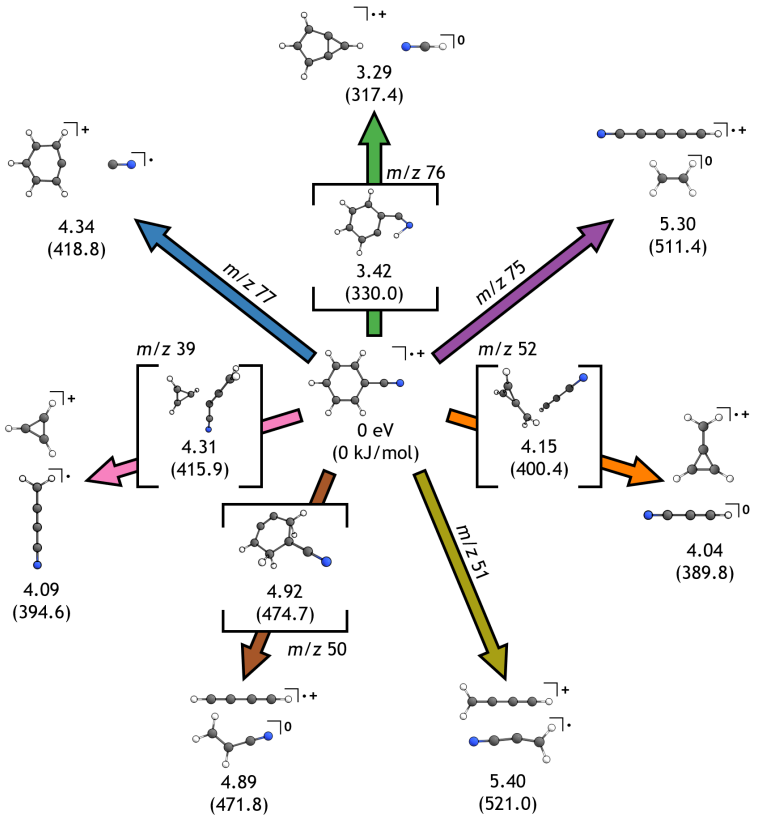

Figure 3.6: Summary of the $C_6H_5CN^{\bullet+}$ potential energy surface. The final neutral and ionic products of each dissociation pathway and their combined energy are shown. The rate-limiting transition states for each pathway are shown within brackets. Pathways without the latter have no reverse barrier. The energies are given in eV and kJ/mol (in parentheses) relative to benzonitrile$^{\bullet+}$.

pathways may make this channel competitive at higher photon energies. Surprisingly, HNC loss does not seem to yield BMB$^{\bullet+}$ based on the PES exploration results.

CH_2CHCN loss (m/z 50 product ion) is the dominant dissociation channel from 18.1 eV onward. With a maximum contribution of about 34% around 19.4 eV. The final products for this channel are found to be diacetylene$^{\bullet+}$ and acrylonitrile, at an energy of 4.89 eV. The rate-limiting step of this pathway is the transition state shown in Fig. 3.6 at an energy of 4.92 eV.

CN loss (m/z 77 product ion) comprises a dissociation channel of benzonitrile$^{\bullet+}$, in which the $CN^{\bullet}$ group is removed without a reverse barrier. This dissociation channel results in the closed-shell phenylium cation and $CN^{\bullet}$ at an energy of 4.34 eV. CN loss is the second most dominant channel in the photon energy range up to 18.1 eV and has a maximum fractional abundance of 25% at a photon energy of 16.8 eV.

HC_3N loss (m/z 52 product ion) shows up in the mass spectra at relatively low photon energy, together with CN and HCN loss. This channel leads to the formation of methylene-cyclopropene$^{\bullet+}$ and cyanoacetylene at 4.04 eV, following the rate-limiting transition state

shown in Fig. 3.6 at an energy of 4.15 eV, which corresponds to the separation of the final two fragments. The HC_3N loss channel reaches its maximal fractional abundance of about 25% at 18.0 eV.

H_2C_4N loss (m/z 39 product ion) results in the formation of cyclopropenium$^+$ (c-$C_3H_3^+$) and $H_2C_4N^\bullet$ at an energy of 4.09 eV. At around 18.5 eV, this channel has its highest fractional abundance of 19%. The rate-limiting step for this channel is the transition state that corresponds to the separation of the two fragments at 4.31 eV. We also considered propargyl cations (l-$C_3H_3^+$) as a possible fragment, but the energy was 1.16 eV higher than c-$C_3H_3^+$.

H_2C_3N loss (m/z 51 product ion) leads to the formation of $H_2C_4H^+$ and cyanovinyl$^\bullet$. The final fragments are formed without a reverse barrier, at an energy of 5.40 eV. The formation of the two fragments is also the rate-limiting step of this pathway. Contribution of the H_2C_3N loss channel does not reach its maximum within the investigated photon energy range.

C_2H_4 loss (m/z 75 product ion) occurs at the highest photon energy and it also has the smallest contribution to the breakdown diagram of benzonitrile. Similar to H_2C_3N loss, the C_2H_4 loss breakdown curve does not reach a maximum within the investigated photon energy range. Cyanodiacetylene$^{\bullet+}$ ($HC_5N^{\bullet+}$) and ethylene (C_2H_4) fragments are formed at an energy of 5.30 eV without a reverse barrier. Among the observed parallel channels, this is the only one where the nitrogen atom stays in the fragment cation. However, $H_2CN^\bullet$ loss is also feasible, leading to the isobaric c-$C_6H_3^+$ fragment at a computed energy of 5.31 eV without a reverse barrier. Its contribution to the m/z 75 peak cannot be ruled out based on the energetics and the expected kinetics, but Rap *et al.* (2023) assigned the m/z 75 peak as cyanodiacetylene$^{\bullet+}$ based on IRPD spectroscopy after 50 eV electron ionization. Therefore, we consider ethylene loss to be dominant in the m/z 75 channel.

3.3.4 Modeling the breakdown diagram and TOF mass spectra

The experimental data are modeled using the miniPEPICO program utilizing RRKM theory to fit the breakdown diagram as well as TOF spectra to extract dissociation barriers (Sztáray *et al.* 2010). Rate-limiting transition states shown in Fig. 3.6 (**TS1**, **TS15**, **TS22** and **TS30** in appendix 3.A.3) are used as the input for the model and their calculated energies and harmonic frequencies serve as initial guess to calculate the transition state number of states and for the dissociation barrier to fit the experimental data. The pathways leading to products at m/z 77, 75 and 51 exhibit no reverse barrier. The barrier therefore corresponds to the dissociation reaction energy. The initial set of harmonic frequencies were obtained after constrained optimization with the bond breaking coordinate fixed at an arbitrary bond length of 4.6 Å. The vibrational mode with the imaginary frequency was checked to make sure that it corresponds to the dissociation coordinate. The model was found to be rather insensitive with respect to the barrier to m/z 76 formation. This is because the kinetic shift, i.e. the excess energy needed to reach fragmentation rates compatible with the residence time in the ionization and acceleration regions, is large, and the rate curve is already flat in the energy range where fragmentation is observed. Therefore, it can be extrapolated to a wide range of input energies by altering the harmonic frequencies of the transition state. Hence, we kept the barrier to HCN loss fixed at the calculated CBS-QB3 transition state energy of 3.42 eV, and employed the statistical fit solely to address the parallel channels and obtain their barriers.

The statistical fit to the experimental breakdown diagram of benzonitrile is shown in Fig. 3.5 and representative fits to the experimental TOF mass spectra are shown in Fig. 3.4. The optimized dissociation barriers are listed in Table 3.1 relative to the energy of the benzonitrile cation and compared with the calculation results.

The relaxed barriers to the m/z 77 and 75 channels are within 0.23 eV of the computed value, which is indicative of the combined uncertainty of the semi-rigid fit, as the barrier

Table 3.1: Dissociation barriers for the primary fragmentation channels of the benzonitrile$^{\bullet+}$ cation. The energies are relative to benzonitrile$^{\bullet+}$. The barrier to m/z 76 formation was kept constant at the calculated CBS-QB3 transition state energy of 3.42 eV (see text).

m/z	Fragment ion	CBS-QB3 (eV)	RRKM model (eV)	ΔE (eV)
77	*c*-$C_6H_5^+$	4.34	4.30	−0.04
76	$C_6H_4^{\bullet+}$	3.42	–	–
75	$HC_5N^{\bullet+}$	5.30	5.53	0.23
52	$C_4H_4^{\bullet+}$	4.15	4.33	0.18
51	$C_4H_3^+$	5.40	5.15	−0.25
50	$C_4H_2^{\bullet+}$	4.92	4.93	0.01
39	*c*-$C_3H_3^+$	4.31	4.41	0.10

to the main, m/z 76 channel has not been relaxed. This is to be expected in light of the large kinetic and competitive shifts. The good agreement between calculation and fit is likely only coincidental for the m/z 50 and 39 channels. Furthermore, calculations in previous works have also come to the conclusion that the final products assumed in this work for the m/z 51 channel, with the largest discrepancy of −0.25 eV, are likely the energetically most favorable (Peverati *et al.* 2016; Johansen *et al.* 2019). This makes us confident that the potential energy surface presents a good approximation of the fragmentation processes and energetics.

3.4 Discussion and conclusions

The ionization and dissociative ionization of benzonitrile were investigated by i^2PEPICO spectroscopy at the VUV beamline of the Swiss Light Source. We could clearly assign the origin ionization transitions to the $\widetilde{X}^+$ and $\widetilde{B}^+$ electronic states of the benzonitrile cation in the TPES and made a tentative assignment of the $\widetilde{C}^+$ electronic state. The Franck–Condon simulated spectra of the assigned states capture the experimental data but post-FC effects, such as lifetime broadening due to strong coupling between electronic states, are clearly seen in the energy range of the electronically excited states of the cation, affecting the unresolved $\widetilde{A}^+$ state the most. From the TPES, the adiabatic ionization energy of the $\widetilde{X}^+$, $\widetilde{B}^+$ and $\widetilde{C}^+$ states is determined to be (9.72 ± 0.02), (11.85 ± 0.03) and (12.07 ± 0.04) eV, respectively, with the third being a tentative assignment.

The seven lowest energy dissociative photoionization channels of benzonitrile are found to occur in parallel via the loss of a $CN^{\bullet}$, HCN, C_2H_4, HC_3N, $H_2C_3N^{\bullet}$, CH_2CHCN and $H_2C_4N^{\bullet}$ fragment, forming *c*-$C_6H_5^+$, $C_6H_4^{\bullet+}$, $HC_5N^{\bullet+}$, $C_4H_4^{\bullet+}$, $C_4H_3^+$, $C_4H_2^{\bullet+}$ and *c*-$C_3H_3^+$, respectively. The breakdown diagram in conjunction with PES calculations helped reveal dissociation channels albeit with limited isomer-specificity. Dissociation barriers were also derived by an RRKM model with the HCN loss anchored to the computational value of 3.42 eV for HCN loss. This yielded optimized barriers of 4.30 eV (CN loss), 5.53 eV (C_2H_4 loss), 4.33 eV (HC_3N loss), 5.15 eV (H_2C_3N loss), 4.93 eV (CH_2CHCN loss) and 4.41 eV (H_2C_4N loss).

In a recent study on the electron-induced dissociative ionization of benzonitrile (Rap *et al.* 2023), HCN/HNC loss was found to be the major dissociation channel at an electron ionization energy of 15 eV, in agreement with our results. Our PEPICO experiments and the electron ionization IRPD experiments by Rap *et al.* (2023) are complementary, thanks to internal energy selection in the former and spectroscopic assignment of the ionic fragments in the latter. Thus, the $C_6H_4^{\bullet+}$ fragment, resulting from HCN/HNC loss, could be determined to be *ortho*-benzyne$^{\bullet+}$ and BMB$^{\bullet+}$. The *ortho*-benzyne$^{\bullet+}$ fragment is the major contributor to the IRPD spectrum. The HCN loss pathway found in this work, however, shows the BMB$^{\bullet+}$, likely in combination with the *meta*-benzyne$^{\bullet+}$ isomer, to be the main fragment

at low internal energies. Since the work of Rap *et al.* (2023) is performed at 15 eV electron energy, the dominance of the *ortho*-benzyne$^{\bullet+}$ fragment ion, which lies about 0.3 eV above BMB$^{\bullet+}$, is likely due to faster rising rate constants because of the looser transition state(s) along the fragmentation pathway.

At 50 eV electron energy, Rap *et al.* (2023) report an increase in the m/z 77 and 75 signals. These peaks could be assigned to the phenylium^{+} (*c*-$C_6H_5^{+}$) and cyanodiacetylene$^{\bullet+}$ ($HC_5N^{\bullet+}$) cation, formed via the loss of $CN^{\bullet}$ and C_2H_4, respectively. The IR spectrum of the cyclic $C_6H_3^{+}$ fragment, the likely product of $H_2CN^{\bullet}$ loss and an isobar of $HC_5N^{\bullet+}$, was ruled out as a major contributor to the IRPD spectrum. This is somewhat at odds with the rate-limiting transition states to *c*-$C_6H_3^{+}$ + $H_2CN^{\bullet}$ and $HC_5N^{\bullet+}$ + C_2H_4 being very similar in energy. It is possible that their competition is energy-dependent and both may contribute to the mass spectrum. Based on calculations, we also reveal a lower-lying dissociation pathway to the m/z 75 fragment ion.

Jacovella *et al.* (2022a) carried out investigations on the VUV dissociation of protonated benzonitrile ($C_6H_5CNH^{+}$) and reported photoproducts at m/z 77, 53 and a very minor contribution at m/z 51. These peaks are shifted to higher mass by 1 amu because of the proton carrying the charge, otherwise the dissociation channels show similarities with the mass spectra of benzonitrile$^{\bullet+}$ reported here. Moreover, the m/z 53 was assigned to the 3-methylcyclopropene cation, which is the analogous to our assignment of methylenecyclopropene to the m/z 52 peak.

The dissociative ionization of benzonitrile can also be compared to the isoelectronic phenylacetylene (C_8H_6). Dyakov *et al.* (2020) studied the PES and the 75 eV EI dissociation of phenylacetylene$^{\bullet+}$ and found dissociation pathways that show similarities to those reported here for benzonitrile$^{\bullet+}$. The final product of neutral C_2H_2 loss, which would be the equivalent of HCN loss for benzonitrile$^{\bullet+}$, was found to be *meta*-benzyne$^{\bullet+}$, which is similar to the BMB$^{\bullet+}$ fragment formed from HCN loss. Prior to the loss of C_2H_2, phenylacetylene$^{\bullet+}$ isomerizes to benzocyclobutadiene$^{\bullet+}$. The isomerization is likely to originate via an ancillary intermediate state, of which the first transition state is comparable to the rate-limiting step of the HCN loss pathway found in this work and the HCN/HNC loss pathway suggested by Rap *et al.* (2023) The calculated energy of this transition state from phenylacetylene$^{\bullet+}$ is 3.33 eV (321 kJ/mol) (Dyakov *et al.* 2020) relative to the cation, which is 0.09 eV lower in energy than the 3.42 eV calculated for the rate-limiting step of HCN loss for benzonitrile$^{\bullet+}$. Indicating that the inclusion of a cyano group instead of a CCH group on a phenyl ring increases the energy required for neighbouring H atom migration towards the respective groups. The inhibition of H atom migration due to the cyano group substitution of a CCH group was also observed by Bouwman *et al.* (2018) in the study on the formation of naphthalene and quinoline from the reaction of phenyl with vinylacteylene and acrylonitrile, respectively.

3.4.1 Astrophysical implications

Ion and radical-driven chemistry thrives in the harsh environment of the atmosphere of Titan, where high-energy photons, electrons and ions are present (Vuitton *et al.* 2007). The mass spectra obtained from the Ion and Neutral Mass Spectrometer (INMS) onboard the Cassini spacecraft have shown that a rich variety of both neutral and cationic molecules play an important role in the atmosphere's chemical processes (Waite *et al.* 2007; Vuitton *et al.* 2007; Kunde *et al.* 1981). Some of the more abundant ions and molecules are also identified in this work as dissociation fragments of benzonitrile$^{\bullet+}$. Since benzonitrile is calculated to be a component of the atmosphere of Titan (Loison *et al.* 2019; Khare *et al.* 1981), the dissociation pathways of benzonitrile$^{\bullet+}$ characterized in this work should be considered as new photofragmentation routes in these models. Expanding this suggestion to the ISM, the fragments and pathways identified in this work should also be included in astrochemical models describing regions where benzonitrile may be exposed to energetic radiation that leads to dissociation of the cation.

Three of the pathways identified in this work (formation of ions of m/z 77, 75 and 51) proceed without a reverse barrier. Traversing these pathways in the opposite direction hence could yield benzonitrile$^{\bullet+}$, thus leading to the following association reactions:

$$c\text{-}C_6H_5{}^+ + CN^\bullet \longrightarrow C_6H_5CN^{\bullet+} \tag{3.2}$$

$$HC_5N^{\bullet+} + C_2H_4 \longrightarrow C_6H_5CN^{\bullet+} \tag{3.3}$$

$$C_4H_3{}^+ + H_2C_3N^\bullet \longrightarrow C_6H_5CN^{\bullet+}. \tag{3.4}$$

All fragments except for $H_2C_3N^\bullet$ are likely present in Titan's atmosphere (Vuitton *et al.* 2007), suggesting that association reactions 3.2 and 3.3 could be driving the formation of benzonitrile in the atmosphere of Titan. Both C_2H_4 and HC_5N are already detected as neutral species in the ISM (McGuire 2022). For example, ionizing radiation could create $HC_5N^{\bullet+}$ which can subsequently react with C_2H_4, thus forming benzonitrile$^{\bullet+}$. Therefore, benzonitrile$^{\bullet+}$ could potentially be formed in the ISM via the association reaction 3.3. When benzonitrile$^{\bullet+}$ is indeed formed via one of the association reactions, its excess energy will possibly be released through IR emission or subsequent dissociation, likely following the pathways discussed herein. If the latter transpires, benzonitrile$^{\bullet+}$ could be considered as a "hub cation", thus linking these species by association and dissociation reactions, thanks to the parallel branching to numerous, highly stable fragments with comparable branching ratios.

Acknowledgements

JB acknowledges the Netherlands Organisation for Scientific Research (Nederlandse Organisatie voor Wetenschappelijk Onderzoek, NWO) for a Vidi grant (grant number 723.016.006). This work was carried out on the Dutch national e-infrastructure with the support of SURF Cooperative (EINF-5273 and EINF-2645). DS acknowledges support by the PRIME programme of the German Academic Exchange Service (DAAD) with funds from the German Federal Ministry of Education and Research (BMBF). The i^2PEPICO experiments were performed at the VUV beamline at the Swiss Light Source. We also wish to thank Patrick Ascher for technical assistance.

3.A Appendices

These appendices contain further information to chapter 3. First, an overview TPES of benzonitrile is presented. Next, the geometries of the $\widetilde{X}^+$, $\widetilde{B}^+$ and $\widetilde{C}^+$ excited states are shown with the bond lengths and angles, together with their Cartesian coordinates. Finally, a detailed description of the potential energy surface (PES) is provided.

3.A.1 TPES overview

The full threshold photoelectron spectrum of benzonitrile spanning the energy range from 9.5 to 14.0 eV is shown in Fig. 3.7.

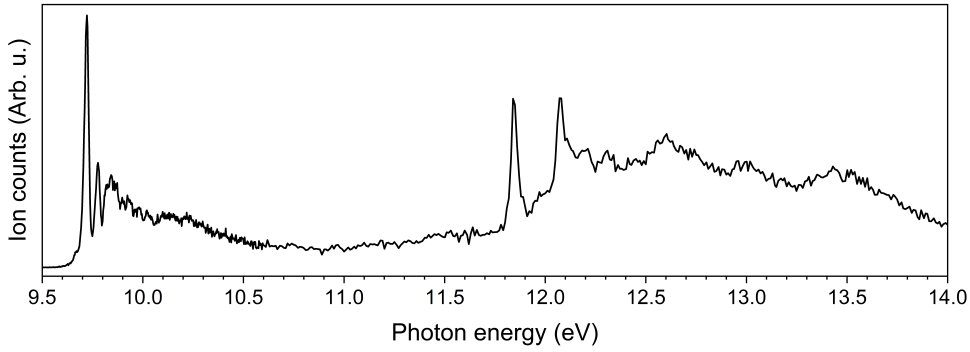

Figure 3.7: Threshold photoelectron spectrum of benzonitrile for the energy range of 9.5 to 14.0 eV.

3.A.2 Benzonitrile excited state structures and their Cartesian coordinates

In this section the Cartesian coordinates of the $\widetilde{X}^+$, $\widetilde{B}^+$ and $\widetilde{C}^+$ excited states that are used to simulate the TPES data are provided together with the bond lengths and angles. The structures were optimized using the ωB97XD/6-311++G(d,p) method.

Fig. 3.8 shows the geometry of the neutral ground state of benzonitrile. The structure is of C_{2v} symmetry. The Cartesian coordinates of this state are presented in Table 3.2.

Fig. 3.9 shows the geometry of the $\widetilde{X}^+$ ground state of benzonitrile cation. The structure is of C_{2v} symmetry, similar to neutral benzonitrile. The Cartesian coordinates of this state are presented in Table 3.3 .

The geometry of the second excited state of the benzonitrile cation, the $\widetilde{B}^+$ state, is shown in Fig. 3.10. Most notably, compared to the $\widetilde{X}^+$ state, the phenyl ring is compressed perpendicular to the principal axis, thereby elongating the ring along this axis. Nevertheless, the structure remains in C_{2v} symmetry. Cartesian coordinates of the $\widetilde{B}^+$ state are presented in Table 3.4.

Lastly, Fig. 3.11 shows the geometry of the $\widetilde{C}^+$ state of benzonitrile. A significant structural change compared to the ground state ion is visible. The most apparent change is that the CN group now has a 179.66° angle. This, along with other structural changes, gives the geometry a C_s symmetry. The Cartesian coordinates of the $\widetilde{C}^+$ state are presented in Table 3.5 .

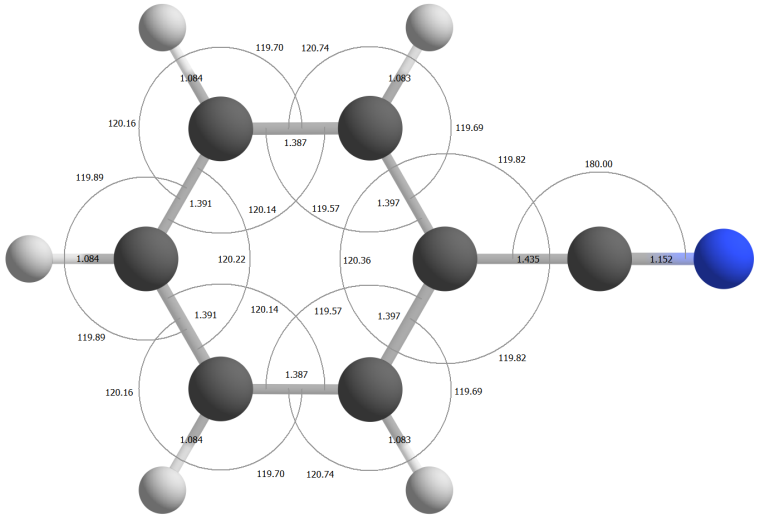

Figure 3.8: Molecular structure of the neutral ground state of benzonitrile accompanied with the bond lengths in Å and bond angles in degrees.

Table 3.2: Cartesian coordinates of the molecular structure of the neutral ground state of benzonitrile.

Atom	Coordinates		
	x	y	z
C	0.000000	1.205814	−1.477156
C	0.000000	1.211771	−0.090012
C	0.000000	0.000000	−2.170236
H	0.000000	2.145173	0.459703
C	0.000000	0.000000	0.604488
C	0.000000	−1.205830	−1.477156
H	0.000000	−2.144650	−2.018109
C	0.000000	−1.211750	−0.090024
H	0.000000	−2.145189	0.459703
C	0.000000	0.000000	2.039246
N	0.000000	0.000000	3.190878
H	0.000000	0.000000	−3.254222
H	0.000000	2.144634	−2.018109

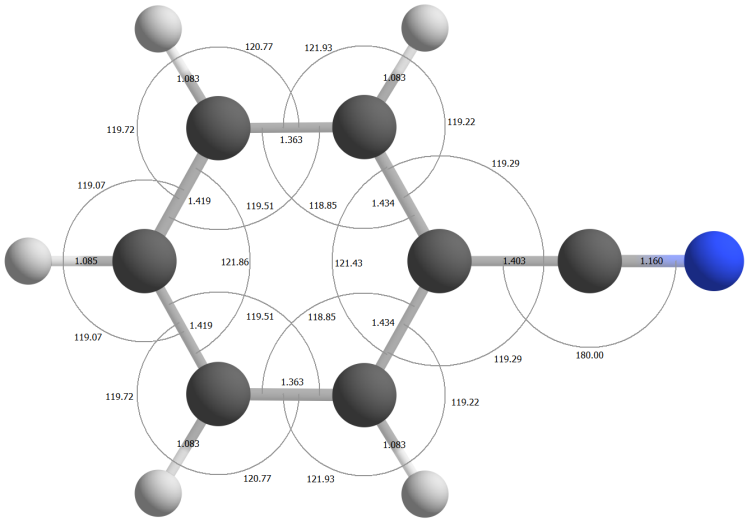

Figure 3.9: Molecular structure of the $\widetilde{X}^{+}$ excited state of benzonitrile accompanied with the bond lengths in Å and bond angles in degrees.

Table 3.3: Cartesian coordinates of the molecular structure of the cationic ground state of benzonitrile.

Atom	Coordinates		
	x	y	z
C	0.000000	1.240442	−1.458870
C	0.000000	1.250888	−0.095564
C	0.000000	0.000000	−2.148443
H	0.000000	2.174662	0.470353
C	0.000000	0.000000	0.605973
C	0.000000	−1.240442	−1.458870
H	0.000000	−2.166581	−2.019942
C	0.000000	−1.250888	−0.095564
H	0.000000	−2.174662	0.470353
C	0.000000	0.000000	2.009291
N	0.000000	0.000000	3.169308
H	0.000000	0.000000	−3.233685
H	0.000000	2.166581	−2.019942

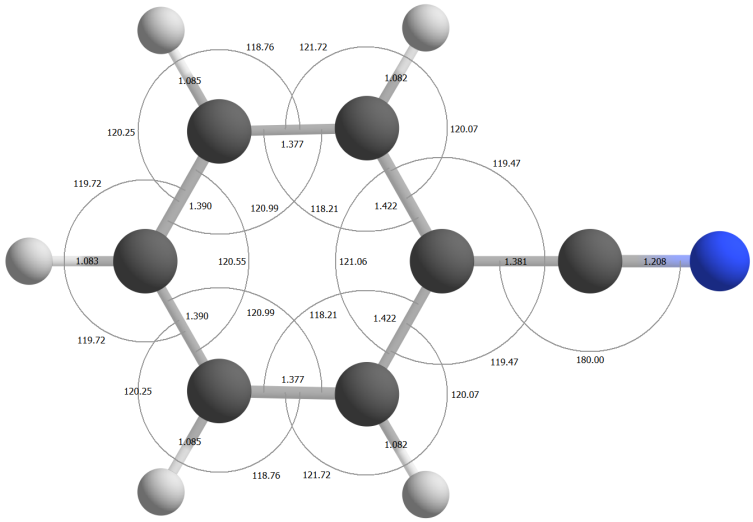

Figure 3.10: Molecular structure of the $\widetilde{B}^{+}$ state of benzonitrile accompanied with the bond lengths in Å and bond angles in degrees.

Table 3.4: Cartesian coordinates of the molecular structure of the $\widetilde{B}^{+}$ state of benzonitrile.

Atom	Coordinates		
	x	y	z
C	0.000000	1.207494	−1.467357
C	0.000000	1.237862	−0.090594
C	0.000000	0.000000	−2.156744
H	0.000000	2.170779	0.457956
C	0.000000	0.000000	0.608925
C	0.000000	−1.207490	−1.467357
H	0.000000	−2.146713	−2.010169
C	0.000000	−1.237872	−0.090570
H	0.000000	−2.170775	0.457956
C	0.000000	0.000000	1.989875
N	0.000000	0.000000	3.198174
H	0.000000	0.000000	−3.239851
H	0.000000	2.146717	−2.010169

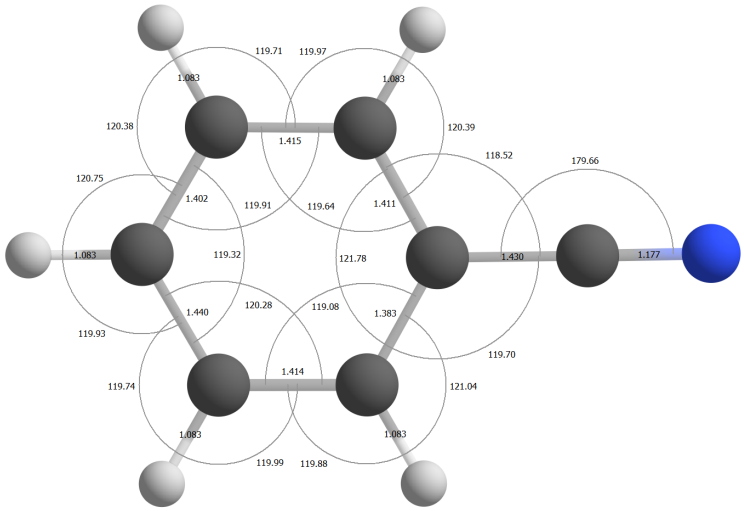

Figure 3.11: Molecular structure of the $\widetilde{C}^{+}$ state of benzonitrile accompanied with the bond lengths in Å and bond angles in degrees.

Table 3.5: Cartesian coordinates of the molecular structure of the $\widetilde{C}^{+}$ state of benzonitrile.

Atom	Coordinates		
	x	y	z
C	0.000000	1.271570	−1.441290
C	0.000000	1.228442	−0.028106
C	0.000000	0.050584	−2.204940
H	0.000000	2.150541	0.539895
C	0.000000	0.000000	0.606781
C	0.000000	−1.179716	−1.532533
H	0.000000	−2.108556	−2.089848
C	0.000000	−1.210675	−0.117513
H	0.000000	−2.160762	0.403006
C	0.000000	−0.059134	2.035740
N	0.000000	−0.114823	3.211320
H	0.000000	0.090139	−3.287217
H	0.000000	2.225972	−1.953906

3.A.3 Detailed description of the PES

This section gives an in-depth description of the PES presented in chapter 3. To facilitate the description of the isomerization pathways, the carbon atoms are numbered as shown in Fig. 3.12. The pathways will be described in descending order of m/z of the cationic

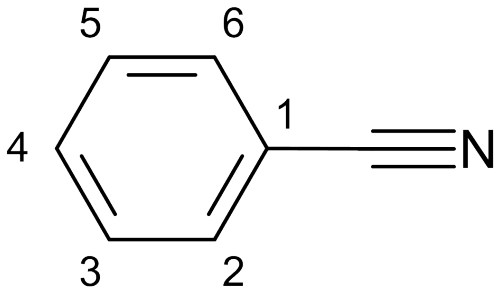

Figure 3.12: The molecular structure of benzonitrile (C_6H_5CN). The carbon atoms in the phenyl ring are numbered

fragments. The colors of the pathways match with the fragments in the breakdown diagram presented in chapter 3. The pathways depicted in black are not considered in the breakdown diagram simulations.

CN loss comprises a benzonitrile dissociation channel in which the CN is removed without a reverse barrier (Fig. 3.13), resulting in the closed-shell phenylium$^+$ and CN$^\bullet$ at an energy of 4.34 eV, with respect to the benzonitrile cation ground state. This channel accounts for about 22% at an energy of 17.0 eV.

HCN loss is the dominant dissociation channel from the onset of dissociation up to about 18.1 eV. At a maximum it accounts for about 98% of the fractional abundance at around 15 eV. This channel leads to the formation of bicyclic *meta*-benzyne$^{\bullet+}$ (BMB$^{\bullet+}$) and HCN. The pathway leading to HCN loss is displayed in Fig. 3.13. The lowest energy path to HCN loss is found to start via **TS1**, which is direct H atom migration from C2 (or by symmetry C6) to the N atom by the at 3.42 eV. This also happens to be the rate-limiting step of the HCN loss channel. Optimizations were also done on the H atom migration to the C atom of the nitrile group, however the resulting structure does not converge and the H atom ends up on the N atom instead. The intermediate state **IN1**, formed over **TS1**, lies at

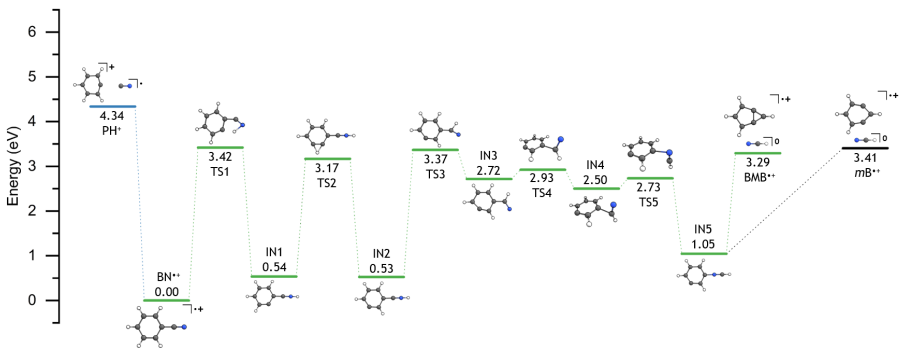

Figure 3.13: The benzonitrile$^{\bullet+}$ potential energy surface resulting in m/z 76 and 77 (blue). Both BMB$^{\bullet+}$ (green) and *meta*-benzyne$^{\bullet+}$ (black) are presented.

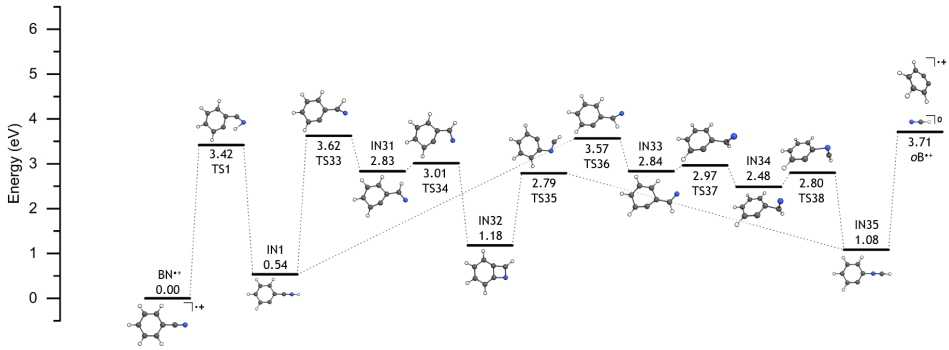

Figure 3.14: The benzonitrile$^{\bullet+}$ potential energy surface resulting in m/z 76 by forming *ortho*-benzyne$^{\bullet+}$. Two possible pathways are presented.

an energy of 0.54 eV. From **IN1**, the H atom bound to C3 migrates to the vacancy on C2 via **TS2** at 3.17 eV, resulting in the intermediate state **IN2** at 0.53 eV. Subsequently, the H atom moves from the nitrogen to the carbon in the nitrile group, creating the HCN moiety. This transition state **TS3** sits at 3.37 eV and gives rise to the intermediate state **IN3** at 2.72 eV. Next, **TS4** located at 2.93 eV is crossed, resulting in **IN4** at 1.05 eV which has an HCN moiety perpendicular to the plane of the phenyl ring. From this intermediate state, the HCN moiety can connected with the nitrogen to C1 via **TS5** at 2.73 eV, resulting in **IN5** which sits at 1.05 eV. This structure exhibits the HCN moiety in-plane with the phenyl ring and the nitrogen atom bound to C1. Finally, bringing C3 and C6 together results in the energetically favorable $C_6H_4{}^{\bullet+}$ structure: BMB$^{\bullet+}$ + HCN at 3.29 eV. Alternatively, by elongating the N-C bond without bringing C3 and C6 closer the fragments *meta*-benzyne$^{\bullet+}$ and HCN are formed at 3.41 eV. Since both energies of the final products are below the energy of rate-limiting transition state **TS1** at 3.42 eV, both cationic fragments are potentially formed.

Ortho-benzyne is energetically unfavourable to be formed at the onset of HCN loss. At higher photon energies, however, *ortho*-benzyne could possibly be formed. The pathway is displayed in Fig. 3.14 and initially follows the same route as BMB$^{\bullet+}$ (or *meta*-benzyne$^{\bullet+}$) formation till **IN1**. Since, *ortho*-benzyne is being formed, no H atom migration in the phenyl ring is necessary. The H atom in the nitrile group moves from the nitrogen to the carbon, creating the HCN moiety. This can proceed in two fashions, namely by the H atom pointing away from the vacancy (**TS33**) or pointing towards it (**TS36**). Following **TS33** at 3.62 eV, we end up at **IN31** with an energy of 2.83 eV. The N atom moves towards the vacancy on the phenyl ring via **TS34** at 3.01 eV and binds to C2, resulting in the bicyclic molecule of **IN32** at 1.18 eV. Subsequently, the bond between C1 and the nitrile group opens which results in **IN35**, where the linear HCN group is bound to C2 with the nitrogen, at 1.08 eV. Separating HCN from the phenyl ring results in out-of-plane *ortho*-benzyne$^{\bullet+}$Kaiser *et al.* (2018) and HCN at 3.71 eV. Following **TS36** at 3.57 eV, we end up at **IN33** with an energy of 2.84 eV. Elongating the bond between C1 and the nitrile group, rotates the nitrile group via **TS37** at 2.97 eV, until it sits in the configuration of **IN34** at 2.48 eV. When the N atom moves towards C1 via **TS38** at 2.80 eV, it binds to C1 causing the C-C bond between C1 and the nitrile group to break, results in **IN35**. Now out-of-plane *ortho*-benzyne$^{\bullet+}$ and HCN can be formed by separating HCN from the phenyl ring. The formation of *ortho*-benzyne$^{\bullet+}$ from benzonitrile$^{\bullet+}$ proceeds without a reverse barrier.

HNC loss, depicted in Fig. 3.15, follows a similar trend as HCN loss for the first few transition and intermediate states. Contrary to HCN loss, at **IN1** and **IN2** the HNC group separates from the molecule without any reconfiguration, resulting in *ortho*- and *meta*-benzyne$^{\bullet+}$ + HNC, respectively.

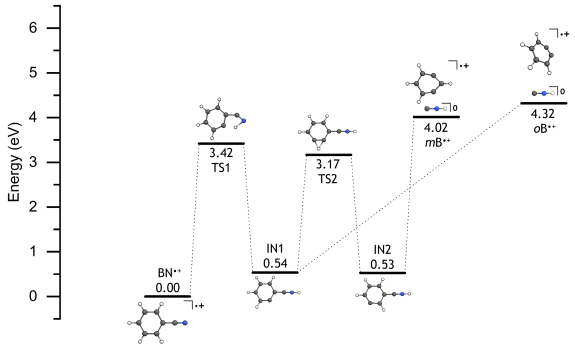

Figure 3.15: The benzonitrile$^{\bullet+}$ potential energy surface resulting in m/z 76 by loss of HNC. Both *meta*- and *ortho*-benzyne$^{\bullet+}$ are presented

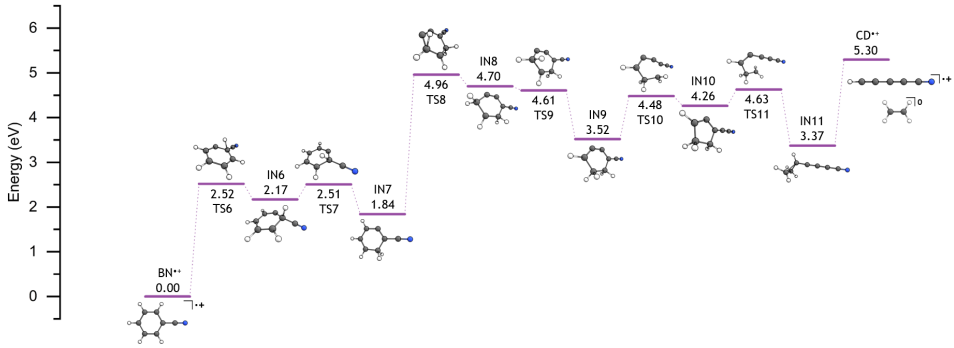

Figure 3.16: The benzonitrile$^{\bullet+}$ potential energy surface resulting in m/z 75 ($HC_5N^{\bullet+}$).

C_2H_4 loss is the only found dissociation pathway to result in a cationic fragment still containing the nitrogen atom of the nitrile group. Within the photon energy range used for this work, this channel does not reach its maximum fractional abundance. The final fragment being formed after dissociation are cyanodiacetylene$^{\bullet+}$ ($HC_5N^{\bullet+}$) and ethylene (C_2H_4). This pathway (shown in Fig. 3.16) starts by hydrogen migration from C6 to C1 via **TS6** at 2.52 eV. The subsequent intermediate state **IN6** sits at an energy of 2.17 eV, with both the migrated hydrogen and the nitrile group sticking out-of-plane. This hydrogen then migrates further to C2 over **TS7** at 2.51 eV, resulting in **IN7** at 1.84 eV with both hydrogens at C2 now sticking out-of-plane. Now, the H atom at C5 migrates to C4, which results in 4.96 eV of required energy to traverse **TS8**, eventually ending up at intermediate state **IN8** at 4.70 eV. One of the hydrogens of C4 then migrates further to C3 via **TS9** at 4.61 eV to form the intermediate state **IN9** at 3.52 eV where two hydrogens sit on both C2 and C3 coming from C6 and C5, respectively. The computed CBS-QB3 energy for **IN8**, however, is slightly higher in comparison to **TS9**. Through the imaginary frequency of **TS9** it is confirmed that it indeed leads to **IN9**. CBS-QB3 utilizes the extrapolated wave function theory in order to determine the electronic energy of a molecular geometry, which is established by density functional theory. This can result in the calculated energy of a transition state being lower than that of the following intermediate state. **TS10** is subsequently traversed at 4.48 eV due to the bond breaking of C1 and C2, thus opening the phenyl ring. However, this ring is closed right after when C2 binds to C6, therefore creating the five-membered ring structure of **IN10** which sits at 4.26 eV. Breaking the bond between C2 and C6 via **TS11** at 4.63 eV, causes the ethylene

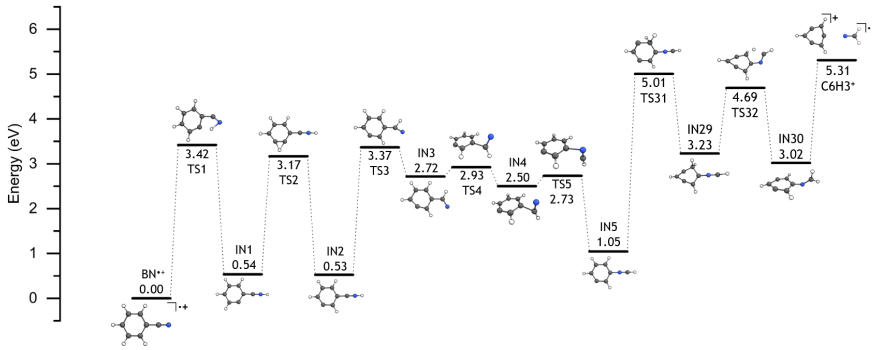

Figure 3.17: The benzonitrile$^{\bullet+}$ potential energy surface resulting in m/z 75 (c-$C_6H_3^+$).

group to rotate and to bind both C2 and C3 to C4, resulting in **IN11** at 3.37 eV. Separating the ethylene group from the molecule, results in the formation of cyanodiacetylene$^{\bullet+}$ and ethylene without a reverse barrier.

H_2CN loss is also considered in this section. The energy of this pathway (shown in Fig. 3.17) is 0.01 eV higher than the pathway to C_2H_4 loss and therefore deemed to not be energetically favourable. However, since the energy difference is so little it will be described here. H_2CN loss follows a similar path as HCN loss up to **IN5**, but from here an H atom migration occurs over **TS31** at 5.01 eV to form the intermediate **IN29** at 3.23 eV. Next, **IN30** at 3.02 eV is formed over **TS32** at 4.69 eV. Lastly, by elongating the C–N bond in **IN30**, c-$C_6H_3^+$ and $H_2CN^{\bullet}$ are obtained at 5.31 eV. This is also the rate-limiting step and takes place without a reverse barier.

HC_3N loss shows up in the mass spectra at m/z 52 at relatively low photon energy (15.7 eV). The lowest pathway found leads to the formation of methylene-cyclopropene$^{\bullet+}$ + cyanoacetylene. The mechanism is shown in Fig. 3.18 and starts by the H atom migration from C4 to C3, crossing **TS12** at 2.20 eV and resulting in **IN12** at 1.82 eV. The next step is to break the C1 and C6 bond and cross **TS13** which is the rate-limiting transition state corresponding to ring opening and is located at 3.69 eV, resulting in **IN13** at 3.13 eV. Next, a rotation takes place around the C2–C3 bond via **TS14** at 3.19 eV, resulting in **IN14** at 3.19 eV. From here, the C2 and C3 bond can be broken by elongation, over **TS15** at 4.14 eV, resulting in methylene-cyclopropene$^{\bullet+}$ and cyanoacetylene at 4.04 eV. **TS15** happens to be the rate-limiting step of this dissociation pathway.

H_2C_3N loss (shown in Fig. 3.18) leads to the formation of $H_2C_4H^+$ at m/z 51 and cyanovinyl$^{\bullet}$, and follows the same initial step as the HC_3N loss channel. However, instead of ring opening from **IN12**, an H atom on C3 moves to C2 via **TS16** at 2.27 eV. This results in **IN15** at 1.82 eV. Next, the H atom on C5 migrates towards the neighboring C6 over **TS17** at an energy of 4.78 eV and results in **IN16** at 4.09 eV. Ring opening at C2 and C3 over **TS18** 5.25 eV results in **IN17** at 3.81 eV. From here, **IN18** at 2.63 eV is formed over **TS19** at 4.15 eV. An internal rotation around the C–C bond takes place via **TS20** at 3.00 eV, resulting in **IN19** at 2.54 eV. By elongating said C–C bond, the transition state **TS21** is traversed at 5.07 eV, which results in **IN20** at 4.74 eV, where the molecule only has an N–H bond. Breaking this bond results in the formation of the two fragments at 5.40 eV.

CH_2CHCN loss is the dominant dissociation channel from 18.1 eV onward and results in an ion with m/z 50 that exhibits a maximum of about 30% around 19.75 eV. The final products found for this channel are diacetylene$^{\bullet+}$ and acrylonitrile, and the pathway is displayed in Fig. 3.18. This loss channel shows a similar lowest energy pathway to H_2C_3N loss. Instead of ring opening from **IN16**, however, it proceeds via hydrogen migration of C6 to C1 over **TS22** at 4.92 eV to form **IN21** at 3.78 eV. Next, bond breaking of C1 and C6

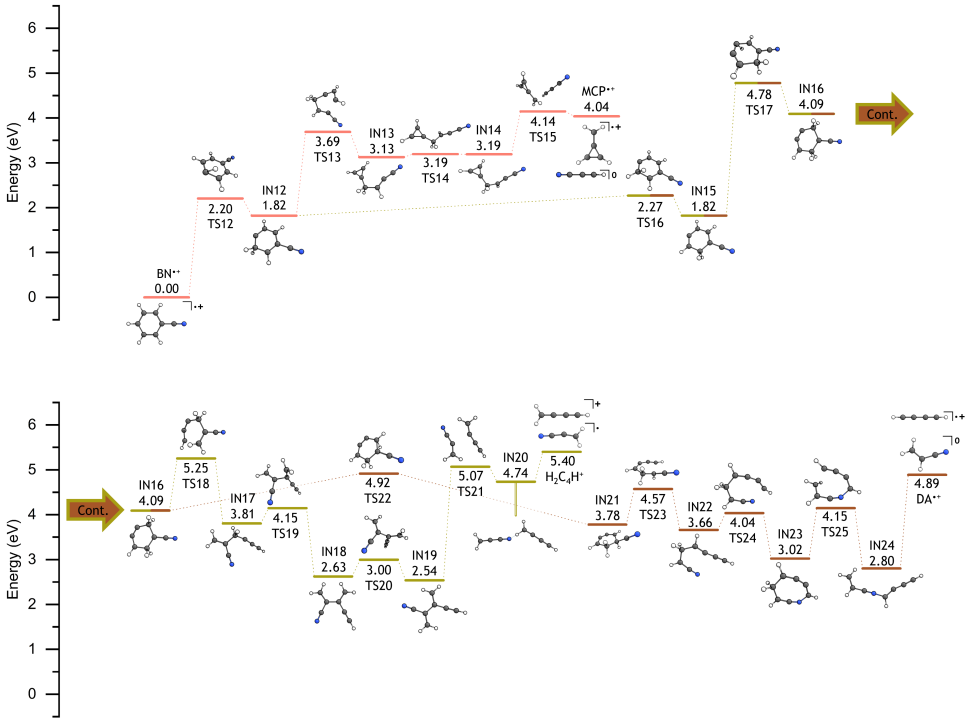

Figure 3.18: The benzonitrile$^{\bullet+}$ potential energy surface leading to the m/z 50 (brown), 51 (yellow), and 52 (orange) fragment ions.

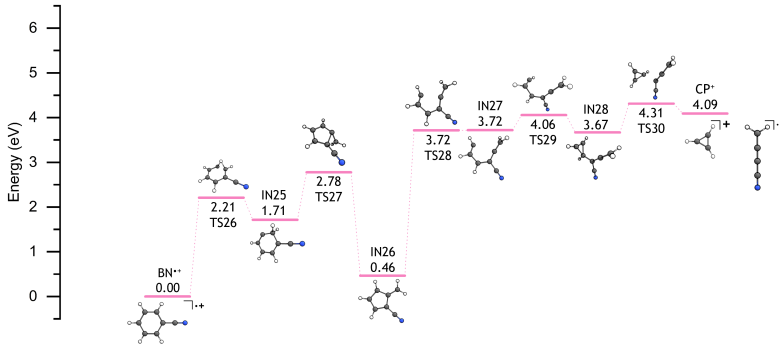

Figure 3.19: The benzonitrile$^{\bullet+}$ potential energy surface resulting in m/z 39.

ensures the ring opening via **TS23** at 4.57 eV resulting in **IN22** at 3.66 eV. Subsequently, a new ring is formed by moving the nitrogen to C6 via **TS24** at 4.04 eV resulting in **IN23** at 3.02 eV. The newly formed ring is broken by the rupture of the C2 and C3 bond via **TS25** at 4.15 eV, forming intermediate **IN24** at 2.80 eV. Finally, breaking the C–N bond results in diacetylene$^{\bullet+}$ and acrylonitrile at 4.89 eV.

H_2C_4N loss results in the formation of cyclopropenium^{+} (at m/z 39) and $H_2C_4N^{\bullet}$ and is schematically displayed in Fig. 3.19. This pathway starts by H atom migration from C5 to C6 over **TS26** at 2.21 eV, resulting in **IN25** at 1.71 eV. Ring compression over **TS27** at 2.78 eV, results in the formation of the five-membered ring intermediate **IN26** at 0.46 eV. Subsequently, ring opening occurs over **TS28** at 3.72 eV and results in intermediate **IN27** at similar energy. Next, **TS29** at 4.06 eV is crossed, resulting in **IN28** at 3.67 eV. Lastly, separating the cyclic species from the H_2C_4N moiety via **TS30** at 4.31 eV, results in cyclopropenium^{+} + $H_2C_4N^{\bullet}$ at 4.09 eV.

3.A.4 (Bicyclic) *meta*-benzyne molecular orbitals

Molecular orbitals (MOs) of *meta*-benzyne and bicyclic *meta*-benzyne (BMB) will be presented in this section. Fig. 3.20 displays the singly occupied MO (SOMO) of the *meta*-benzyne and BMB cations, and the highest occupied MO (HOMO) and HOMO−1 of neutral *meta*-benzyne. The *meta*-benzyne and BMB cation SOMOs are clearly different, and show

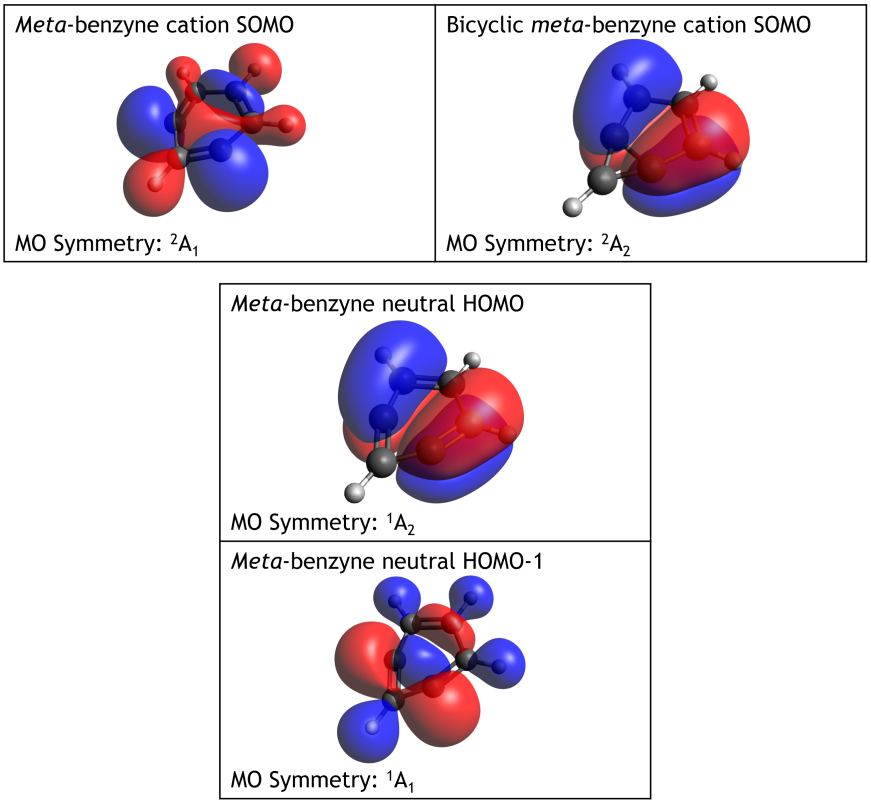

Figure 3.20: The SOMO of the *meta*-benzyne and BMB cations, and the HOMO and HOMO−1 of neutral *meta*-benzyne.

a $^2A_1$ and $^2A_2$ symmetry, respectively. Thus, the two cationic isomers represent two minima with different wave function symmetries and are therefore clearly distinguishable. It seems that ionization out of the neutral HOMO leads to the BMB cation, while ionization out of the HOMO−1 results in the *meta*-benzyne cation.